Thermodynamics of long-chain 1-alkyl-3-methylimidazolium bis(trifluoromethanesulfonyl)imide ionic liquids

Eugene Paulechka[1,2 *], Andrey V. Blokhin[1], Ana S. M. C. Rodrigues[3], Marisa A. A. Rocha[3 ***], Luís M. N. B. F. Santos[3 **]

[1] *Chemistry Faculty, Belarusian State University, Leningradskaya 14, 220030 Mink, Belarus*

[2] *Applied Chemicals and Materials Division, National Institute of Standards and Technology, Boulder, CO 80305-3337, United States*

[3] *CIQ, Departamento de Química e Bioquímica, Faculdade de Ciências da Universidade do Porto, Porto, Portugal*

* To whom correspondence concerning the adiabatic calorimetry should be addressed. E-mail: yauheni.paulechka@nist.gov

** To whom correspondence concerning the vapour-pressure measurements should be addressed. E-mail: lbsantos@fc.up.pt

*** Present address: Technische Thermodynamik, Universität Bremen, Badgasteiner Str. 1, D-28359 Bremen, Germany

Abstract

The heat capacities in the temperature range (5 to 370) K and the parameters of solid-phase phase transitions and fusion were determined for three [$C_n$mim][NTf_2] (n = 10, 14, 16) ILs. The temperature-dependent vapour pressures of [C_{14}mim][NTf_2] and [C_{16}mim][NTf_2] were measured with a Knudsen effusion apparatus combined with a quartz crystal microbalance. Thermodynamic properties of these compounds in the crystal, liquid, and gas states were derived from the obtained data. The results obtained in this work were combined to those available in the literature for the short-chain homologues to discuss regularities in thermodynamic properties of the series. While some properties demonstrate simple linear dependence on the alkyl chain length, a more complicated behaviour with strong non-linearity or a break at n = 6 is observed for others.

1. Introduction

1-Alkyl-3-methylimidazolium bis(trifluoromethanesulfonyl)imides [$C_n$mim][NTf_2] are among the most studied room-temperature ionic liquids (ILs). Most studies and particularly the thermodynamic studies were conducted on the short-chain homologues. Heat capacities for the temperature range 5 K – 370 K and parameters of phase transitions from adiabatic calorimetry have been reported for [$C_n$mim][NTf_2] (n = 2,4,6,8,18) [1] [2] [3] [4] [5] [6]. Most of the heat-capacity values on [C_{18}mim][NTf_2] [5] were presented graphically and, therefore, they are of limited use. Rocha *et al.* [7] used a drop calorimeter [8] to determine heat capacities at T = 298.15 K for [$C_n$mim][NTf_2] (n = 2 to 12). Dzyuba and Bartsch [9] determined parameters of a solid-phase transition and fusion for [C_{10}mim]NTf_2 with DSC. The parameters of fusion were determined by DSC for the liquids with n = 12, 14, 16, 18 [10]

and n = 18, 22 [11]. Therefore, entropy and other thermodynamic functions for the long-chain NTf_2 containing ILs in the condensed state have not been reported.

The vapour pressures have been reported for the compounds with $n \leq 12$ [12], [13]. For series members with longer chains, only enthalpies of vaporization are available [14], [15].

In this work, we report the results of studies on the long-chain [$C_n$mim][NTf_2] ionic liquids by adiabatic calorimetry and the quartz-microbalance Knudsen effusion method. The results are used to calculate thermodynamic properties of these compounds in various phases over wide temperature ranges and to analyse regularities in thermodynamic properties of these ILs.

2. Experimental

2.1. Sample Purification and Characterization

Characteristics of the samples studied are given in table 1. The samples of [C_{10}mim][NTf_2], [C_{14}mim][NTf_2], and [C_{16}mim][NTf_2] used for the vapour-pressure measurements were purchased from IoLiTec with a stated mole fraction purity of better than 0.98. The purity of each ionic liquid was further evaluated with ^{1}H NMR spectra (see Supplementary Material), and all ILs were found to be > 0.99 mass fraction. The halide content was assumed to be that given by the supplier, <100 ppm. [C_{14}mim][NTf_2] and [C_{16}mim][NTf_2] were solid at room temperature and were dried under reduced pressure (< 10 Pa) at 323 K to reduce the presence of water or other volatile contents. Water mass fraction content was found to be below 100×10^{-6} measured in a Metrohm 831 Karl Fischer coulometer using a Hydranal-Coulomat AG from Riedel-de Haën. The ILs were additionally purified by evacuation at T = 533 K under high vacuum ($<10^{-4}$ Pa) inside the Knudsen effusion cell before the vapour-pressure measurements.

The sample of $[C_{14}mim][NTf_2]$ used for calorimetric measurements was provided by Prof. Ya.S. Vygodskii of the A. N. Nesmeyanov Institute of Organoelement Compounds, Russian Academy of Sciences (INEOS RAS). The sample was exposed to a vacuum ($p \approx 1$ Pa) at T = 293 K prior to the measurements. Purities of all samples studied in the adiabatic calorimeter were also determined by fractional melting (figure 1).

The purity of $[C_{10}mim][NTf_2]$ determined by fractional melting is significantly lower than that found with NMR. The fractional melting procedure gives the total amount of impurity species in a sample. If the sample contains an ionic impurity containing uncharged ions (for example, isomeric IL), the purity will be 0.9875 mol fraction that is comparable with the NMR value.

TABLE 1

Provenance and purity of the samples studied.

Abbreviation	Source	Initial mole fraction purity	Purification method	Final fraction purity	Analysis method
$[C_{10}mim][NTf_2]$	IOLITEC	>0.98	Vacuum treatment	0.975 mol	Fractional melting
				>0.99 mass	NMR
$[C_{14}mim][NTf_2]$	IOLITEC	>0.98	Vacuum treatment	>0.99 mass	NMR
	INEOS RAS	N/A	Vacuum treatment	0.982 mol	Fractional melting

$[C_{16}mim][NTf_2]$	IOLITEC	>0.98	Vacuum treatment	0.997 mol	Fractional melting
				>0.99 mass	NMR

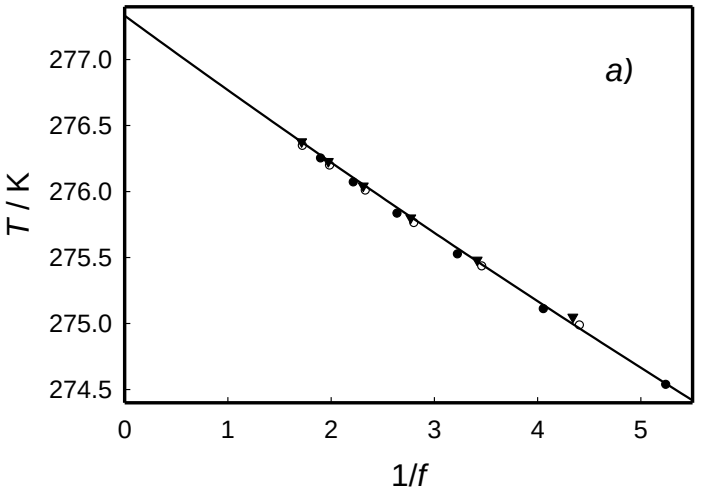

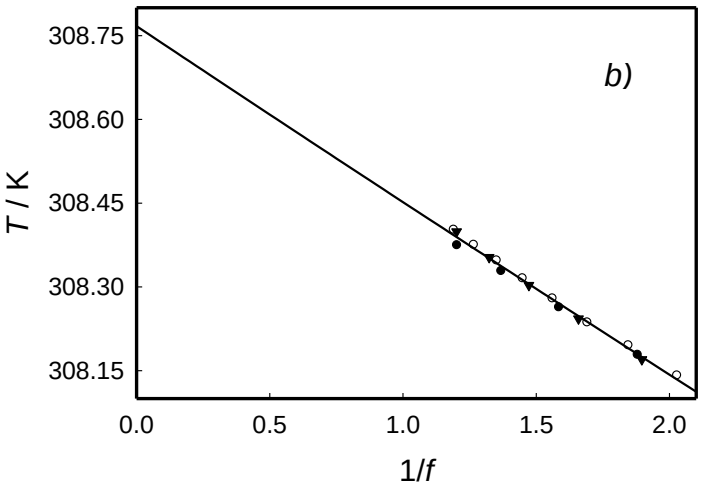

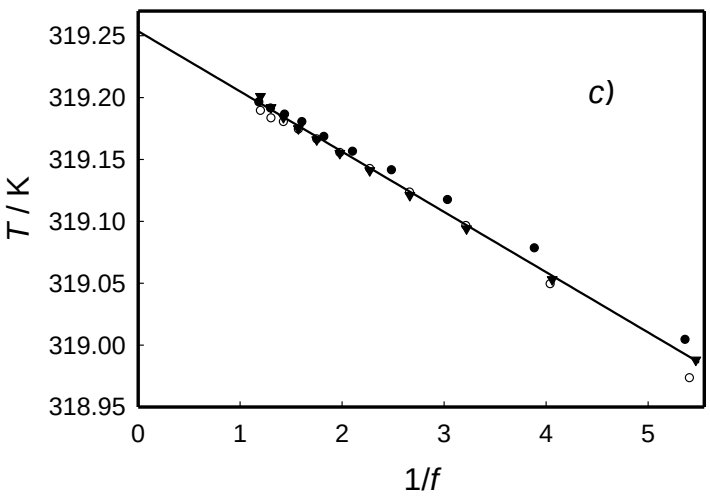

FIGURE 1. Results of fractional melting experiments for (a) $[C_{10}mim][NTf_2]$, (b) $[C_{14}mim][NTf_2]$, and (c) $[C_{16}mim][NTf_2]$, where f is the fraction of the sample in the liquid state and T is the corresponding equilibrium temperature. Various symbols are used for different series of measurements.

2.2. Adiabatic calorimetry

Heat capacity over the temperature range from (5 to 370) K was measured in a TAU-10 adiabatic calorimeter (Termis, Moscow, Russia) [16]. The experimental procedures were elsewhere [2]. The heat capacity of the sample contributed about 0.8 of the total heat capacity of the system near 5 K, and 0.3–0.5 outside the phase transition ranges at 80 K – 370 K. The equilibration times were close to 100 s at the lowest temperatures. At higher temperatures, the equilibration times were typically 300 s – 400 s. In the pre-melting range, the equilibration times to 3900 s were allowed. The expanded uncertainty (0.95 confidence interval) in the heat-capacity measurements was 0.4 % above T = 20 K and 2 % near T = 5 K [2].

The triple-point temperatures T_{fus} and the sample purities were determined with the van't Hoff equation in the form:

$$\ln\left(1+\frac{n_2}{f}\right)=\frac{\Delta_{\mathrm{fus}}H_{\mathrm{m}}}{R}\left(\frac{1}{T_{\mathrm{fus}}}-\frac{1}{T}\right), \qquad (1)$$

where n_2 is the amount of impurity, mole per mole of the main component; f is the fraction melted at temperature T, R = 8.314460 J·K^{-1}·mol^{-1} [17], and $\Delta_{fus}H_m$ is the molar enthalpy of fusion at T_{fus}.

The baselines for the solid-phase transitions and fusion were selected using the following criteria: (i) smooth heat capacity over the ranges of the solid phase transition and the pre-melting range; (ii) concave baseline shape ($dC_p/dT > 0$); (iii) the baseline should involve the minimum heat capacity between the phase transitions.

Sample masses used for the calorimetric measurements were corrected for buoyancy. The reported uncertainties correspond to the 95% confidence interval for the normal distribution (coverage factor k = 2) unless specified otherwise.

2.3. Quartz crystal microbalance Knudsen effusion apparatus

Vapour pressures of the ILs were measured with a Knudsen effusion apparatus combined with a quartz crystal microbalance (KEQCM) described in the literature [18]. This approach allows gravimetric determination of the overall mass loss, as well as monitoring of the effusion rate with the quartz crystal microbalance. In a Knudsen step effusion, the system is kept at high vacuum (< 1×10^{-4} Pa), enabling free effusion of the vapour from the cell, while the oven is kept at a fixed temperature T. The vapour pressure p was calculated for each isothermal step using

$$p = \left(\frac{\mathrm{d}f}{\mathrm{d}t}\right) \cdot \left(\frac{1}{w_0 \cdot A_0 \cdot W}\right) \cdot \left(\frac{2 \cdot \pi \cdot R \cdot T}{M}\right)^{1/2} \qquad (2)$$

where M is the molar mass of the sample, w_0 is the transmission probability factor ($w_0 = \{1 + (l/2r)\}^{-1}$), R is the gas constant, (df/dt) is the rate of change of the resonance frequency of the quartz crystal, and A_0 is the area of the orifice. The overall effective mass sensitivity coefficient, W, is derived from the experimental mass loss for the cell Δm(cell) with

$$W = \left(\frac{\Delta f}{\Delta m(\text{cell})} \right) \tag{3}$$

where Δf is the total change in the crystal's resonance frequency during the experiment.

3. Results

3.1. Condensed State

Experimental heat capacities for the studied ILs are reported in figures 2–4 and in tables S1–S3. The coefficients of polynomials for the liquid heat capacities are listed in table 2. The temperatures and enthalpies of phase transitions in the condensed state are presented in table 3. The corresponding experimental values can be found in tables S4–S9.

The liquid heat capacity of $[C_{10}mim][NTf_2]$ at T = 298.15 K reported by Rocha *et al.* [7] agrees with the current results within 0.04%. The temperatures and enthalpies of phase transitions for $[C_{10}mim][NTf_2]$ measured by DSC [9] are too low by about 5 K and 50%, respectively, relative to the values obtained in this work. The reason of these deviations is unknown. The temperatures and enthalpies of fusion for $[C_{14}mim][NTf_2]$ and $[C_{16}mim][NTf_2]$ also determined by DSC [10] agree with our results within 4 K and 10%, respectively.

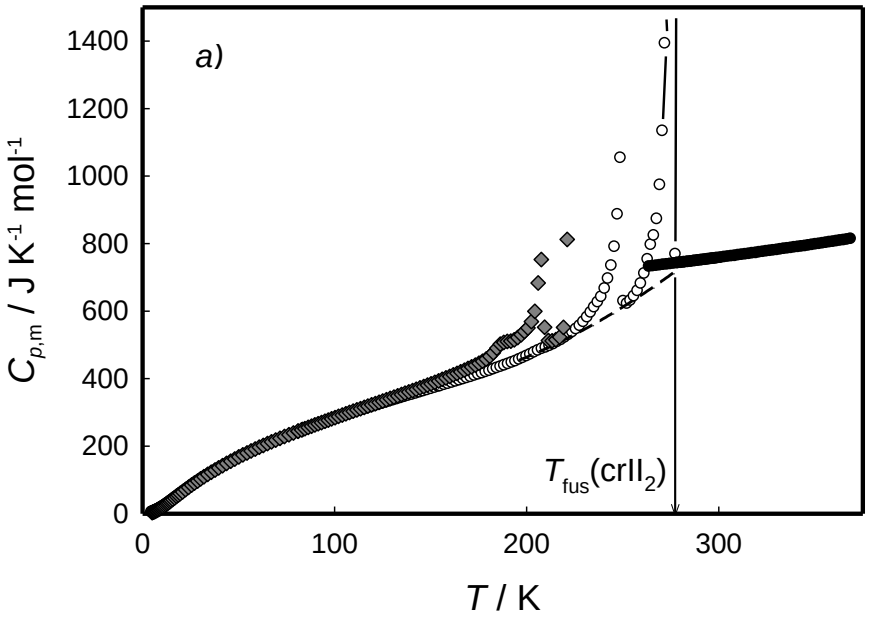

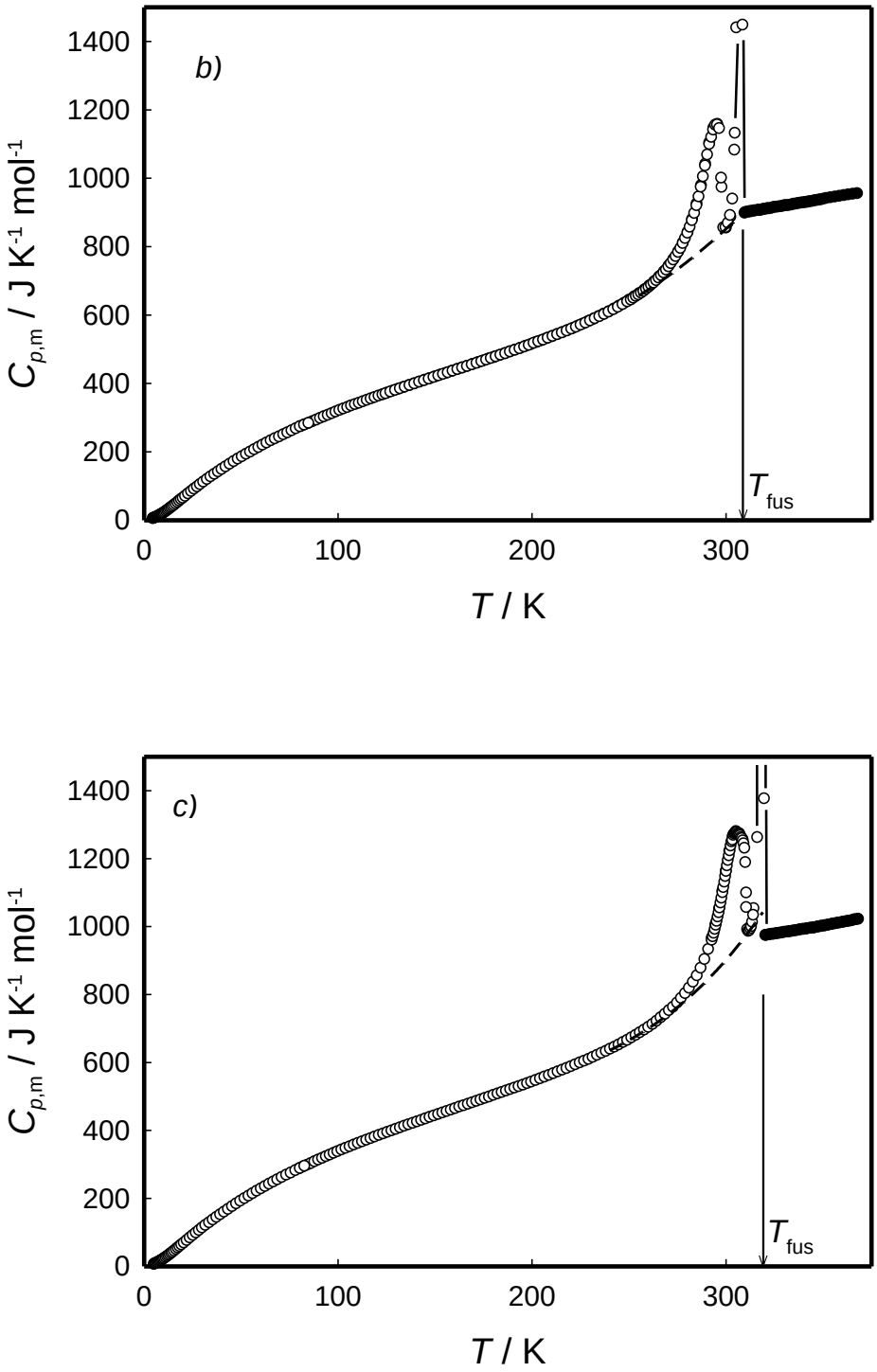

FIGURE 2. Experimental heat capacities of the ILs studied: (a) $[C_{10}mim][NTf_2]$; (b) $[C_{14}mim][NTf_2]$; (c) $[C_{16}mim][NTf_2]$. ●, liquid phase; ○, most stable crystal sequence; grey diamond, metastable crystal sequence I for $[C_{10}mim][NTf_2]$; – – –, baseline for the solid-phase transition and fusion.

TABLE 2

Coefficients for polynomials $C_{p,m}^{o}$ / J·K^{-1}·mol^{-1} = a_0 + a_1(T / K) + a_2(T / K)^2 describing liquid heat capacities of [C$_n$mim][NTf$_2$].

n	a_0	a_1	a_2	T range / K
10	620.04	0.15943	9.8129×10^{-4}	263–370
14 [a]	595.16	0.97520		309–370
16	1085.9	-1.5185	3.6348×10^{-3}	320–370

[a] A preliminary report of heat capacities for the liquid phase for this compound was published earlier [19].

[C$_{10}$mim][NTf$_2$]. Cooling of the liquid from $T \geq 300$ K at an initial rate of about 20 mK·s^{-1} resulted in super-cooling, followed by crystallization near T = 233 K. The phase sequence obtained this way is noted Sequence I throughout the text. To distinguish crystal phases within this sequence, Arabic numeral indices were added starting from 1 for the lowest-temperature phase (for example, crI$_1$).

TABLE 3

Summary of parameters of phase transitions in the condensed state for the ILs studied. [a]

IL	Type of transition	T_{tr} / K	$\Delta_{tr}H_m^{\circ}$ / kJ·mol^{-1}
[C$_{10}$mim][NTf$_2$]	crI$_1$–crI$_2$ [b]	207.3 ± 0.5[c]	
	crII$_1$–crII$_2$	249 ± 1[c]	2.51 ± 0.03[d]
	crII$_2$–l	277.33 ± 0.03	28.67 ± 0.02

$[C_{14}mim][NTf_2]$	crI–crII	295.5 ± 0.4[c]	4.25 ± 0.09
	crII–l	308.77 ± 0.03	45.18 ± 0.04[e]
$[C_{16}mim][NTf_2]$	crI–crII	305.5 ± 0.5[c]	5.34 ± 0.23
	crII–l	319.25 ± 0.03	51.28 ± 0.24

[a] The expanded uncertainty with 0.95 confidence level; [b] metastable sequence; [c] temperature of the heat-capacity maximum; [d] for crystal obtained at T_{an} = 275 K; [e] the melting peak has an additional maximum at T = (307.82 ± 0.05) K.

A sigmoid anomaly was observed for crI_1 in the temperature range 175 K – 192 K (figure 1a). The inflexion point was T = 184 K. This anomaly can also be interpreted as a peak on a rising branch of a subsequent phase transition crI_1–crI_2. Structural studies are needed to reveal the nature of this anomaly. To check reversibility of the described phenomena, the following procedure was used. First, a series of measurements from (78 to 189) K was conducted. Then, the sample was cooled and a new series was performed, which was stopped at 215 K. After that, the sample was cooled again and the measurements were repeated. Heat capacities of the crystal in these three series agreed within the combined uncertainty of the measurements.

Starting from T = 216 K, an exothermal spontaneous process of transformation into polymorphic Sequence II began. The complete transformation took about 12 h, and the maximum temperature reached during this process was T = 233 K.

Sequence II had a non-isothermal solid-phase transition $crII_1$–$crII_2$. A shape of the heat-capacity curve in a region of the phase transition depended on the temperature T_{an} at which the sample was annealed during crystallization (figure 3). At T_{an} = 233 K, a smooth small peak with a maximum at T = (243 ± 1) K was observed. If T_{an} was equal to 275 K, a sharp peak appeared and its maximum shifted to (249 ± 1) K. An intermediate curve was observed

if T_{an} was close to the maximum temperature of the phase transition peak. The enthalpy of this solid-phase transition for the crystal obtained at T_{an} = 275 K was found to be (2.50 ± 0.03) kJ·mol^{-1} (table 2).

Below T = 200 K, the differences in heat capacity of these crystals did not exceed 0.6% and decreased with lowering temperature. However, at higher temperatures the differences became significant. The crystal obtained at T_{an} =275 K was the most stable one. For example, at T = 200 K its enthalpy was (0.9 ± 0.4) kJ·mol^{-1} lower compared to the crystal obtained at T_{an} = 247 K. Similar behaviour has been reported for other [C$_n$mim][NTf$_2$] ILs [1], [20].

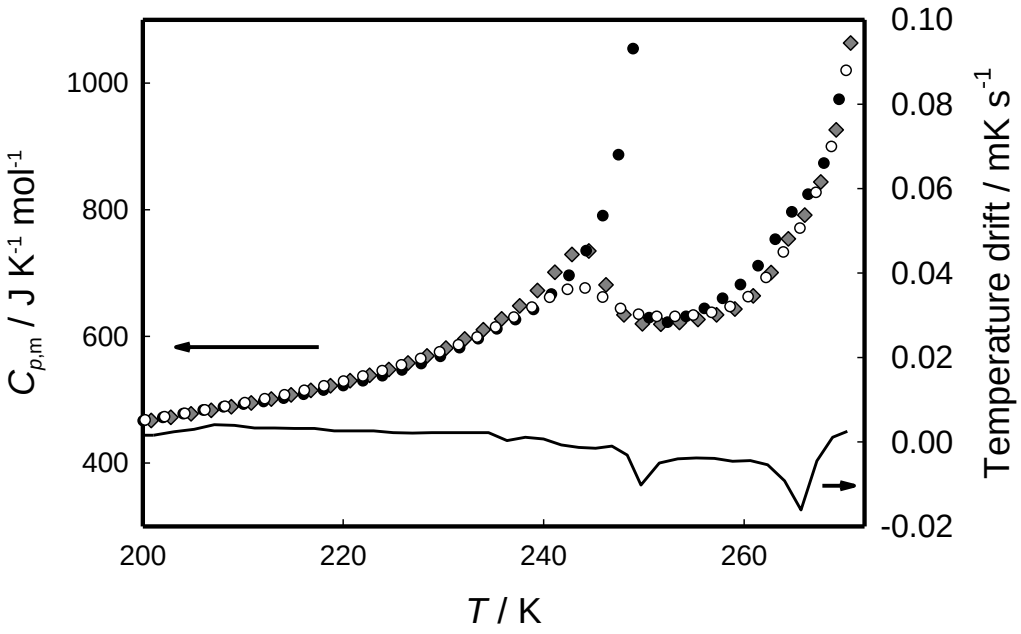

FIGURE 3. Experimental heat capacities and temperature drifts in calorimetric measurements in a region of a solid-phase transition and pre-melting for crII sequence of [C$_{10}$mim][NTf$_2$]: ○, T_{an} = 233 K; gray diamonds, T_{an} = 247 K; ●, T_{an} = 275 K. Temperature drifts at (475 to 600) s after termination of the heating period are shown for the crystals annealed at T_{an} = 275 K.

Crystals of Sequence II obtained at T_{an} = 275 K had an admixture of 1.8% sequence I, as evaluated from the excess enthalpy in the region 195 K – 211 K. Heat capacity in this region was corrected for the presence of Sequence I. The effect of the admixture on heat capacity of crII was negligible for T < 195 K. Above T = 211 K the effect could not be evaluated directly since the experimental data for Sequence I were not available. We estimate that differences in heat capacity of the two sequences will not exceed 10% and the effect of the admixture will be negligible at higher temperatures.

Duration of a calorimetric experiment was normally chosen to have the sample in thermal equilibrium at the end. In this case, the temperature drift of the calorimeter is close to zero at the end of the experiment. In the region of a phase transition, the relaxation time often increases. If duration of a calorimetric experiment is not increased, the temperature drifts become negative or positive depending on the process. In the temperature region shown in figure 3, two peaks in the temperature drifts are observed. The first one corresponds to the maximum heat capacity during the $crII_1$–$crII_2$ transition. The second peak reveals an endothermic process with a maximum at T = 266 K. Surprisingly, only minor changes are observed in the heat-capacity curve close to this peak. The sample contained an admixture of Sequence I and no exothermic effect was observed, which could be assigned to the crI→crII transformation. Therefore, we propose that this peak may correspond to melting of crI_2. Further studies are required to confirm this hypothesis.

$[C_{14}mim][NTf_2]$. Cooling of the liquid sample resulted in crystallization at $T \approx$ 290 K. A solid-1phase transition and fusion were detected (table 3). To confirm reversibility of the transition, the trial series was conducted where measurements were stopped at T = 301 K, that is just after the transition, the sample was cooled to 230 K, and the measurements were repeated. In both cases, the experimental data were indistinguishable within their uncertainties.

The melting peak had an extra maximum 0.8 K below the melting temperature of the sample (figure 4). This maximum of unknown nature was reproducible for the crystals obtained with annealing temperatures T_{an} = (304.5 to 307.4) K with annealing times varying from (0 to 17) h. No detectable changes in heat capacity and parameters of phase transitions were found for the crystals thus obtained. Deconvolution of the melting peak into two separate phase-transition peaks could not be achieved. In calculation of thermodynamic properties, we assumed that the whole peak corresponds to the melting at T_{fus} = 308.77 K. Also, the range of f^{-1} in the fractional-melting analysis was narrower compared to other studied ILs (figure 1).

The triple-point temperature for $[C_{14}mim][NTf_2]$ is consistent with the preliminary value reported [19], while the enthalpies of fusion differ significantly. The differences are caused by change in the baseline heat capacity of crystal used in the calculations. The procedure used for generation of baselines in this work is preferable since it allowed us to make consistent data treatment for all studied compounds.

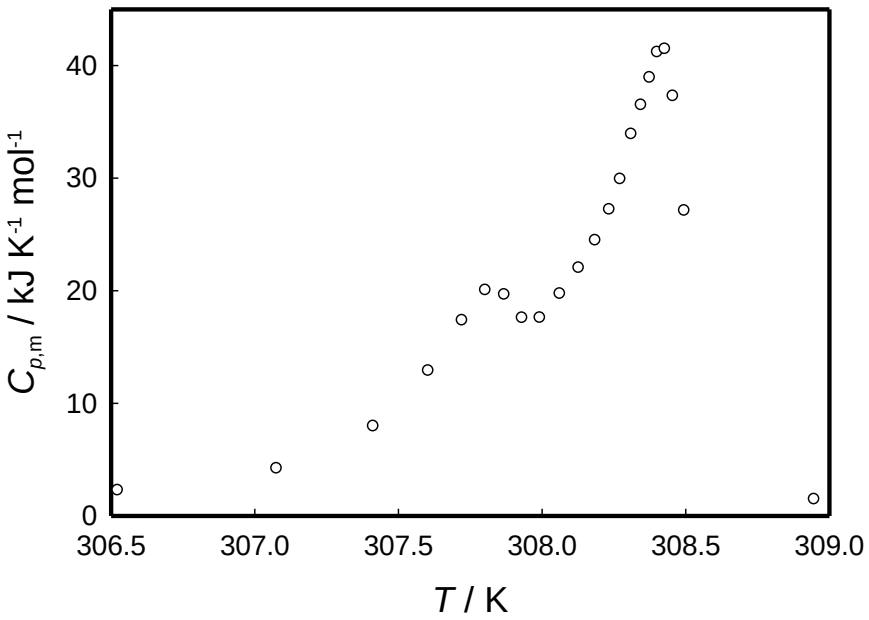

FIGURE 4. Measured heat capacities in the pre-melting region for crI of [C_{14}mim][NTf_2]. Uncertainties are large due to long equilibration times that precluded high-precision measurements in this region.

[C_{16}mim][NTf_2]. On cooling, the liquid crystallized at $T \approx 305$ K. This compound had a non-isothermal solid-phase transition close to its melting point. To confirm reversibility of the transition, the trial series was conducted where measurements were stopped at $T = 314$ K, that is just above the transition, the sample was cooled to 200 K, and the measurements were repeated. In both cases, the experimental data agreed within their uncertainties. The heat capacities were also indistinguishable for the crystal obtained with no annealing after crystallization and the crystal annealed during 4 h at $T = 319$ K.

Thermodynamic functions for the studied compounds in the condensed state are reported in Tables 4–6. Heat capacities of the crystals were extrapolated to $T = 0$ K using the empirical equation

$$C_{p,\mathrm{m}} = D_3(\theta_\mathrm{D}/T) + 3E(\theta_\mathrm{E}/T) \qquad (4)$$

where $D_3(\theta_\mathrm{D} / T)$ is the Debye heat-capacity function for three degrees of freedom and $E(\theta_\mathrm{E} / T)$ is the Einstein heat capacity function for one degree of freedom. The θ_D and θ_E determined from the experimental values are presented in table S10.

The thermodynamic functions, including those in the non-isothermal phase transition regions, were calculated using the smoothed heat capacities. Within narrow ranges where the heat capacities changed abruptly, numerical integration of the experimental heat capacities was applied. The baselines were used for the calculations only in the pre-melting ranges.

TABLE 4

Thermodynamic properties for [C_{10}mim][NTf_2] in the condensed state (p^o = 0.1 MPa).[a]

$\frac{T}{\mathrm{K}}$	$\frac{C_{p,\mathrm{m}}}{\mathrm{J \cdot K^{-1} \cdot mol^{-1}}}$	$\frac{S^\circ_\mathrm{m}}{\mathrm{J \cdot K^{-1} \cdot mol^{-1}}}$	$\frac{\Delta_0^T H^\circ_\mathrm{m}/T}{\mathrm{J \cdot K^{-1} \cdot mol^{-1}}}$	$\frac{-\Delta_0^T G^\circ_\mathrm{m}/T}{\mathrm{J \cdot K^{-1} \cdot mol^{-1}}}$
		Sequence I (metastable)		
0	0	0	0	0
5	3.41 ± 0.07	1.17 ± 0.02	0.87 ± 0.02	0.29 ± 0.03
10	18.31 ± 0.27	7.58 ± 0.13	5.49 ± 0.10	2.09 ± 0.17
15	39.12 ± 0.37	18.82 ± 0.27	13.13 ± 0.18	5.69 ± 0.32
20	61.00 ± 0.24	33.09 ± 0.36	22.38 ± 0.22	10.71 ± 0.42
25	82.14 ± 0.33	48.99 ± 0.43	32.23 ± 0.23	16.75 ± 0.49
30	102.0 ± 0.4	65.74 ± 0.50	42.23 ± 0.25	23.52 ± 0.56
35	120.1 ± 0.5	82.86 ± 0.56	52.09 ± 0.28	30.77 ± 0.63
40	136.7 ± 0.5	100.0 ± 0.6	61.64 ± 0.31	38.35 ± 0.70
45	152.5 ± 0.6	117.0 ± 0.7	70.85 ± 0.34	46.13 ± 0.78
50	167.6 ± 0.7	133.9 ± 0.8	79.79 ± 0.37	54.08 ± 0.85
60	194.8 ± 0.8	166.9 ± 0.9	96.74 ± 0.43	70.1 ± 1.0
70	219.4 ± 0.9	198.8 ± 1.0	112.5 ± 0.5	86.3 ± 1.1
80	242.1 ± 1.0	229.6 ± 1.2	127.3 ± 0.5	102.3 ± 1.3
90	263.4 ± 1.1	259.3 ± 1.3	141.3 ± 0.6	118.1 ± 1.4
100	283.9 ± 1.1	288.1 ± 1.4	154.5 ± 0.6	133.6 ± 1.5
110	304.1 ± 1.2	316.2 ± 1.5	167.2 ± 0.7	149.0 ± 1.6
120	323.7 ± 1.3	343.5 ± 1.6	179.4 ± 0.7	164.0 ± 1.8
130	343.2 ± 1.4	370.1 ± 1.7	191.3 ± 0.8	178.9 ± 1.9
140	363.3 ± 1.5	396.3 ± 1.8	202.8 ± 0.8	193.5 ± 2.0

150	384.3 ± 1.5	422.1 ± 1.9	214.2 ± 0.9	207.9 ± 2.1
160	406.8 ± 1.6	447.6 ± 2.0	225.5 ± 0.9	222.0 ± 2.2
170	431.2 ± 1.7	473.0 ± 2.1	236.9 ± 1.0	236.1 ± 2.3
180	462.6 ± 1.9	498.4 ± 2.2	248.5 ± 1.0	249.9 ± 2.4
190	510.3 ± 2.0	524.9 ± 2.3	261.2 ± 1.1	263.7 ± 2.6
200	546.2 ± 2.2	551.8 ± 2.4	274.3 ± 1.1	277.4 ± 2.7
210	513.0 ± 2.1	581.9 ± 2.6	291.0 ± 1.2	290.9 ± 2.8

Sequence II

0	0	0	0	0
5	3.41 ± 0.07	1.18 ± 0.02	0.88 ± 0.02	0.30 ± 0.03
10	17.29 ± 0.25	7.33 ± 0.13	5.27 ± 0.09	2.06 ± 0.16
15	36.94 ± 0.34	17.93 ± 0.26	12.45 ± 0.17	5.48 ± 0.31
20	58.37 ± 0.23	31.50 ± 0.35	21.26 ± 0.21	10.24 ± 0.40
25	79.32 ± 0.32	46.80 ± 0.41	30.79 ± 0.22	16.00 ± 0.46
30	98.90 ± 0.40	63.01 ± 0.47	40.54 ± 0.24	22.48 ± 0.53
35	116.6 ± 0.5	79.61 ± 0.54	50.16 ± 0.27	29.45 ± 0.60
40	132.9 ± 0.5	96.26 ± 0.61	59.50 ± 0.30	36.76 ± 0.68
50	163.2 ± 0.7	129.2 ± 0.7	77.27 ± 0.36	51.97 ± 0.82
60	190.4 ± 0.8	161.4 ± 0.9	93.90 ± 0.42	67.55 ± 0.96
70	214.9 ± 0.9	192.7 ± 1.0	109.5 ± 0.5	83.2 ± 1.1
80	237.4 ± 0.9	222.8 ± 1.1	124.1 ± 0.5	98.8 ± 1.2
90	258.5 ± 1.0	252.0 ± 1.2	137.8 ± 0.6	114.2 ± 1.4
100	278.7 ± 1.1	280.3 ± 1.3	150.9 ± 0.6	129.4 ± 1.5
110	297.7 ± 1.2	307.8 ± 1.5	163.4 ± 0.7	144.4 ± 1.6
120	315.8 ± 1.3	334.4 ± 1.6	175.3 ± 0.7	159.1 ± 1.7

130	333.3 ± 1.3	360.4 ± 1.7	186.8 ± 0.8	173.6 ± 1.8
140	350.5 ± 1.4	385.8 ± 1.8	197.9 ± 0.8	187.8 ± 1.9
150	367.5 ± 1.5	410.5 ± 1.9	208.6 ± 0.9	201.9 ± 2.0
160	384.7 ± 1.5	434.8 ± 2.0	219.1 ± 0.9	215.7 ± 2.2
170	402.3 ± 1.6	458.6 ± 2.1	229.4 ± 0.9	229.3 ± 2.3
180	420.7 ± 1.7	482.1 ± 2.2	239.5 ± 1.0	242.7 ± 2.4
190	440.9 ± 1.8	505.4 ± 2.2	249.5 ± 1.0	255.9 ± 2.5
200	463.2 ± 1.9	528.6 ± 2.3	259.7 ± 1.1	268.9 ± 2.6
210	489.1 ± 2.0	551.8 ± 2.4	270.0 ± 1.1	281.9 ± 2.7
220	519.8 ± 2.1	575.2 ± 2.5	280.6 ± 1.1	294.7 ± 2.8
230	569.2 ± 2.3	599.3 ± 2.6	292.0 ± 1.2	307.4 ± 2.9
240	651.3 ± 2.6	625.2 ± 2.7	305.1 ± 1.2	320.1 ± 3.0
249	1053 ± 4	653.6 ± 2.8	322.0 ± 1.3	331.6 ± 3.1
252	619.2 ± 2.5	662.4 ± 2.9	327.0 ± 1.3	335.4 ± 3.2
260	648.7 ± 2.6	682.3 ± 3.0	336.5 ± 1.4	345.8 ± 3.2
270	687.6 ± 2.8	707.5 ± 3.1	348.8 ± 1.4	358.7 ± 3.4
277.33	717.5 ± 2.9	726.3 ± 3.1	358.1 ± 1.4	368.2 ± 3.4
		Liquid		
277.33	739.7 ± 3.0	829.8 ± 3.5	461.7 ± 1.9	368.2 ± 4.0
280	741.6 ± 3.0	836.9 ± 3.6	464.3 ± 1.9	372.6 ± 4.0
290	748.8 ± 3.0	863.1 ± 3.7	474.0 ± 1.9	389.1 ± 4.1
298.15	754.8 ± 3.0	883.9 ± 3.8	481.6 ± 1.9	402.3 ± 4.2
300	756.2 ± 3.0	888.6 ± 3.8	483.3 ± 1.9	405.3 ± 4.2
310	763.8 ± 3.1	913.5 ± 3.9	492.2 ± 2.0	421.3 ± 4.4
320	771.5 ± 3.1	937.9 ± 4.0	500.8 ± 2.0	437.0 ± 4.5

330	779.5 ± 3.1	961.7 ± 4.1	509.1 ± 2.0	452.6 ± 4.6
340	787.7 ± 3.2	985.1 ± 4.2	517.2 ± 2.1	467.9 ± 4.7
350	796.0 ± 3.2	1008 ± 4	525.1 ± 2.1	483.0 ± 4.7
360	804.6 ± 3.2	1031 ± 4	532.7 ± 2.1	497.9 ± 4.8
370	813.4 ± 3.3	1053 ± 4	540.2 ± 2.2	512.6 ± 4.9

[a] Uncertainties reported in the table are the expanded uncertainty with 0.95 level of confidence. The expanded uncertainty for temperature is $U_c(T)$ = 0.02 K.

TABLE 5

Thermodynamic properties for $[C_{14}mim][NTf_2]$ in the condensed state (p^o = 0.1 MPa).[a]

$\frac{T}{\mathrm{K}}$	$\frac{C_{p,\mathrm{m}}}{\mathrm{J \cdot K^{-1} \cdot mol^{-1}}}$	$\frac{S^\circ_{\mathrm{m}}}{\mathrm{J \cdot K^{-1} \cdot mol^{-1}}}$	$\frac{\Delta_0^T H^\circ_{\mathrm{m}}/T}{\mathrm{J \cdot K^{-1} \cdot mol^{-1}}}$	$\frac{-\Delta_0^T G^\circ_{\mathrm{m}}/T}{\mathrm{J \cdot K^{-1} \cdot mol^{-1}}}$
		Crystal		
0	0	0	0	0
5	3.43 ± 0.07	1.17 ± 0.02	0.88 ± 0.02	0.30 ± 0.03
10	17.94 ± 0.26	7.53 ± 0.13	5.44 ± 0.10	2.09 ± 0.16
15	38.56 ± 0.36	18.57 ± 0.27	12.93 ± 0.18	5.64 ± 0.32
20	61.41 ± 0.25	32.77 ± 0.36	22.18 ± 0.21	10.59 ± 0.42
25	84.18 ± 0.34	48.94 ± 0.43	32.32 ± 0.23	16.62 ± 0.48
30	105.9 ± 0.4	66.22 ± 0.49	42.79 ± 0.26	23.44 ± 0.56
35	126.4 ± 0.5	84.11 ± 0.57	53.29 ± 0.29	30.82 ± 0.63
40	145.8 ± 0.6	102.3 ± 0.6	63.66 ± 0.32	38.62 ± 0.71
45	164.1 ± 0.7	120.5 ± 0.7	73.81 ± 0.35	46.70 ± 0.79
50	181.5 ± 0.7	138.7 ± 0.8	83.71 ± 0.39	54.99 ± 0.87
60	213.6 ± 0.9	174.7 ± 0.9	102.7 ± 0.5	71.95 ± 1.03

70	242.6 ± 1.0	209.8 ± 1.1	120.7 ± 0.5	89.15 ± 1.19
80	269.2 ± 1.1	244.0 ± 1.2	137.6 ± 0.6	106.4 ± 1.3
90	293.7 ± 1.2	277.1 ± 1.3	153.6 ± 0.6	123.5 ± 1.5
100	316.7 ± 1.3	309.3 ± 1.5	168.8 ± 0.7	140.5 ± 1.6
110	338.4 ± 1.4	340.5 ± 1.6	183.2 ± 0.8	157.3 ± 1.8
120	358.8 ± 1.4	370.8 ± 1.7	197.0 ± 0.8	173.8 ± 1.9
130	378.6 ± 1.5	400.3 ± 1.8	210.2 ± 0.9	190.1 ± 2.0
140	397.8 ± 1.6	429.1 ± 1.9	222.9 ± 0.9	206.1 ± 2.1
150	416.6 ± 1.7	457.2 ± 2.1	235.2 ± 1.0	221.9 ± 2.3
160	435.3 ± 1.7	484.6 ± 2.2	247.1 ± 1.0	237.5 ± 2.4
170	454.1 ± 1.8	511.6 ± 2.3	258.8 ± 1.0	252.8 ± 2.5
180	473.1 ± 1.9	538.1 ± 2.4	270.1 ± 1.1	268.0 ± 2.6
190	492.5 ± 2.0	564.2 ± 2.5	281.3 ± 1.1	282.9 ± 2.7
200	512.7 ± 2.1	589.9 ± 2.6	292.4 ± 1.2	297.6 ± 2.8
210	533.6 ± 2.1	615.5 ± 2.7	303.4 ± 1.2	312.1 ± 3.0
220	556.0 ± 2.2	640.8 ± 2.8	314.3 ± 1.3	326.5 ± 3.1
230	580.3 ± 2.3	666.0 ± 2.9	325.4 ± 1.3	340.7 ± 3.2
240	607.6 ± 2.4	691.3 ± 3.0	336.5 ± 1.4	354.8 ± 3.3
250	639.3 ± 2.6	716.7 ± 3.1	348.0 ± 1.4	368.7 ± 3.4
260	677.5 ± 2.7	742.5 ± 3.2	359.9 ± 1.4	382.6 ± 3.5
270	734.5 ± 2.9	769.1 ± 3.3	372.7 ± 1.5	396.4 ± 3.6
280	830.5 ± 3.3	797.3 ± 3.4	387.1 ± 1.6	410.2 ± 3.8
290	1046 ± 4	829.7 ± 3.5	405.6 ± 1.6	424.1 ± 3.9
295.5	1155 ± 5	850.6 ± 3.6	418.8 ± 1.7	431.9 ± 4.0
298.15	971.6 ± 3.9	860.5 ± 3.7	424.9 ± 1.7	435.6 ± 4.0

300	851.8 ± 3.4	866.0 ± 3.7	427.7 ± 1.7	438.3 ± 4.1
308.77	898.6 ± 3.6	891.2 ± 3.8	440.4 ± 1.8	450.8 ± 4.2
		Liquid		
308.77	896.2 ± 3.6	1037 ± 4	586.7 ± 2.4	450.8 ± 5.0
310	897.4 ± 3.6	1041 ± 4	587.9 ± 2.4	453.1 ± 5.0
320	907.2 ± 3.6	1070 ± 5	597.8 ± 2.4	471.9 ± 5.1
330	917.0 ± 3.7	1098 ± 5	607.3 ± 2.4	490.5 ± 5.2
340	926.7 ± 3.7	1125 ± 5	616.5 ± 2.5	508.7 ± 5.3
350	936.5 ± 3.7	1152 ± 5	625.5 ± 2.5	526.7 ± 5.5
360	946.2 ± 3.8	1179 ± 5	634.3 ± 2.5	544.5 ± 5.6
370	956.0 ± 3.8	1205 ± 5	642.9 ± 2.6	562.0 ± 5.7

[a] Uncertainties reported in the table are the expanded uncertainty with 0.95 level of confidence. The expanded uncertainty for temperature is $U_c(T)$ = 0.02 K.

TABLE 6

Thermodynamic properties for $[C_{16}mim][NTf_2]$ in the condensed state (p^o = 0.1 MPa).[a]

$\frac{T}{\mathrm{K}}$	$\frac{C_{p,\mathrm{m}}}{\mathrm{J \cdot K^{-1} \cdot mol^{-1}}}$	$\frac{S^\circ_{\mathrm{m}}}{\mathrm{J \cdot K^{-1} \cdot mol^{-1}}}$	$\frac{\Delta_0^T H^\circ_{\mathrm{m}}/T}{\mathrm{J \cdot K^{-1} \cdot mol^{-1}}}$	$\frac{-\Delta_0^T G^\circ_{\mathrm{m}}/T}{\mathrm{J \cdot K^{-1} \cdot mol^{-1}}}$
		Crystal		
0	0	0	0	0
5	3.58 ± 0.07	1.23 ± 0.02	0.92 ± 0.02	0.31 ± 0.03
10	18.51 ± 0.27	7.81 ± 0.14	5.63 ± 0.10	2.18 ± 0.17
15	39.66 ± 0.37	19.15 ± 0.27	13.32 ± 0.18	5.84 ± 0.33
20	63.15 ± 0.25	33.76 ± 0.37	22.83 ± 0.22	10.94 ± 0.43
25	86.78 ± 0.35	50.40 ± 0.44	33.26 ± 0.24	17.14 ± 0.50

30	109.7 ± 0.4	68.27 ± 0.51	44.11 ± 0.26	24.16 ± 0.57
35	131.4 ± 0.5	86.83 ± 0.58	55.05 ± 0.29	31.78 ± 0.65
40	151.7 ± 0.6	105.7 ± 0.7	65.87 ± 0.33	39.84 ± 0.74
45	171.3 ± 0.7	124.7 ± 0.7	76.50 ± 0.36	48.21 ± 0.82
50	190.0 ± 0.8	143.7 ± 0.8	86.92 ± 0.40	56.82 ± 0.91
60	224.6 ± 0.9	181.5 ± 1.0	107.0 ± 0.5	74.5 ± 1.1
70	255.9 ± 1.0	218.5 ± 1.1	126.1 ± 0.5	92.4 ± 1.2
80	284.5 ± 1.1	254.6 ± 1.3	144.1 ± 0.6	110.4 ± 1.4
90	310.8 ± 1.2	289.6 ± 1.4	161.2 ± 0.7	128.4 ± 1.5
100	335.5 ± 1.3	323.6 ± 1.5	177.4 ± 0.7	146.2 ± 1.7
110	358.8 ± 1.4	356.7 ± 1.7	192.9 ± 0.8	163.9 ± 1.8
120	380.5 ± 1.5	388.9 ± 1.8	207.6 ± 0.9	181.3 ± 2.0
130	401.4 ± 1.6	420.2 ± 1.9	221.7 ± 0.9	198.5 ± 2.1
140	421.7 ± 1.7	450.7 ± 2.0	235.3 ± 1.0	215.4 ± 2.3
150	441.5 ± 1.8	480.4 ± 2.2	248.4 ± 1.0	232.1 ± 2.4
160	461.2 ± 1.8	509.6 ± 2.3	261.0 ± 1.1	248.5 ± 2.5
170	480.8 ± 1.9	538.1 ± 2.4	273.4 ± 1.1	264.7 ± 2.6
180	500.5 ± 2.0	566.1 ± 2.5	285.5 ± 1.2	280.7 ± 2.8
190	520.4 ± 2.1	593.7 ± 2.6	297.3 ± 1.2	296.4 ± 2.9
200	540.8 ± 2.2	621.0 ± 2.7	309.0 ± 1.2	312.0 ± 3.0
210	562.3 ± 2.2	647.9 ± 2.8	320.5 ± 1.3	327.3 ± 3.1
220	585.0 ± 2.3	674.5 ± 2.9	332.0 ± 1.3	342.5 ± 3.2
230	609.3 ± 2.4	701.1 ± 3.0	343.5 ± 1.4	357.5 ± 3.3
240	635.6 ± 2.5	727.5 ± 3.1	355.2 ± 1.4	372.4 ± 3.5
250	665.4 ± 2.7	754.1 ± 3.3	367.0 ± 1.5	387.1 ± 3.6

260	700.6 ± 2.8	780.8 ± 3.4	379.1 ± 1.5	401.8 ± 3.7
270	745.5 ± 3.0	808.1 ± 3.5	391.8 ± 1.6	416.3 ± 3.8
280	806.6 ± 3.2	836.2 ± 3.6	405.4 ± 1.6	430.8 ± 3.9
290	909.7 ± 3.6	866.1 ± 3.7	420.9 ± 1.7	445.3 ± 4.1
298.15	1084 ± 4	893.4 ± 3.8	436.3 ± 1.8	457.1 ± 4.2
300	1146 ± 5	900.3 ± 3.8	440.5 ± 1.8	459.9 ± 4.2
305.5	1274 ± 5	922.5 ± 3.9	454.5 ± 1.8	468 ± 4.3
310	1229 ± 5	941.0 ± 4.0	466.3 ± 1.9	474.7 ± 4.4
319.25	1044 ± 4	971.3 ± 4.1	482.6 ± 1.9	488.7 ± 4.6
		Liquid		
319.25	972 ± 4	1132 ± 5	643.2 ± 2.6	488.7 ± 5.4
320	972 ± 4	1134 ± 5	644.0 ± 2.6	490.2 ± 5.4
330	981 ± 4	1164 ± 5	654.1 ± 2.6	510.2 ± 5.6
340	990 ± 4	1194 ± 5	663.8 ± 2.7	529.8 ± 5.7
350	1000 ± 4	1222 ± 5	673.2 ± 2.7	549.2 ± 5.8
360	1010 ± 4	1251 ± 5	682.5 ± 2.7	568.3 ± 5.9
370	1022 ± 4	1279 ± 5	691.5 ± 2.8	587.1 ± 6.0

[a] Uncertainties reported in the table are the expanded uncertainty with 0.95 level of confidence. The expanded uncertainty for temperature is $U_c(T) = 0.02$ K.

3.2. Vaporization

The experimental vapour pressures obtained from the average of five independent (T, p) experiments are listed in table 7 and depicted in the graphical representation as $\ln(p/\mathrm{Pa}) = f(\mathrm{K}/T)$ in figure 5. The experimental results were fitted using the integrated form of the Clausius-Clapeyron equation

$$\ln(p/p^{\circ}) = a - b/T \qquad (5)$$

where a and b are the fitted parameters, p° = 0.1 MPa.

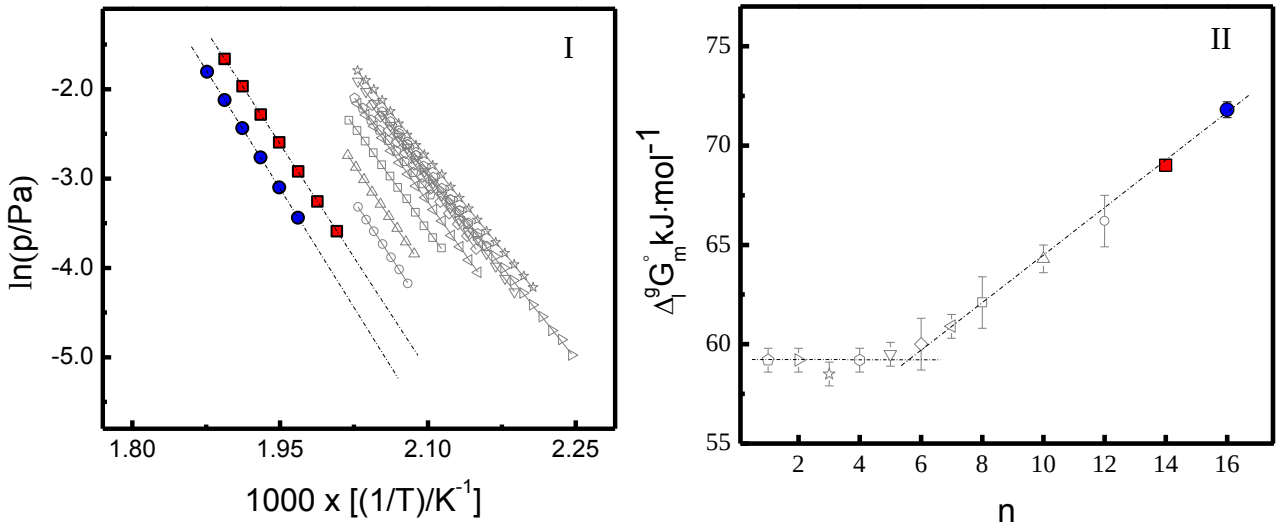

FIGURE 5. Vapour pressures of [C$_n$mim][NTf$_2$] ILs, (I). Graphical representation of the standard molar Gibbs energy of vaporization $\Delta_l^g G_m^o(\theta = 460.0\ \mathrm{K})$ as a function of the number of carbons n in the alkyl side chain of the cation, (II). This work: ■ [C$_{14}$mim] [NTf$_2$]; ● [C$_{16}$mim] [NTf$_2$]. Literature data [12], [13]. ⬠ [C$_1$mim][NTf$_2$]; ▷ [C$_2$mim][NTf$_2$]; ☆ [C$_3$mim][NTf$_2$]; ⬡ [C$_4$mim][NTf$_2$]; ▽ [C$_5$mim][NTf$_2$]; ◇ [C$_6$mim][NTf$_2$]; ◁ [C$_7$mim][NTf$_2$]; □ [C$_8$mim][NTf$_2$]; △ [C$_{10}$mim][NTf$_2$]; ○ [C$_{12}$mim][NTf$_2$].

TABLE 7

Experimental results of vapour pressure p and temperature T for the studied ILs, obtained with the quartz crystal microbalance Knudsen effusion apparatus. [a]

$[C_{14}mim][NTf_2]$			$[C_{16}mim][NTf_2]$		
T / K	p / Pa	Δp / Pa	T / K	p / Pa	Δp / Pa
498.07	0.0276	0.0058	508.07	0.0321	0.0025
503.06	0.0385	-0.0034	513.07	0.0450	-0.0030
508.05	0.0539	0.0002	518.07	0.0631	0.0003
513.05	0.0745	0.0020	523.07	0.0875	0.0008
518.04	0.1018	-0.0063	528.06	0.1197	-0.0035
523.05	0.1397	0.0004	533.07	0.1644	-0.0028
528.05	0.1898	0.0056			

[a] $\Delta p = p - p_{calc}$, where p_{calc} is calculated from the Clarke and Glew equation (8) with the parameters given in Table 9. Expanded uncertainties, U, are $U(T) = 0.02$ K, $U(p) = (0.001 + 0.05 \cdot p)$ Pa, the 0.95 confidence level ($k \approx 2$).

Table 8 presents the parameters of the Clausius–Clapeyron equation derived from the experimental (T, p) results, the standard deviations, the mean temperature $\langle T \rangle$, and the pressure at the mean temperature $p(\langle T \rangle)$. The standard molar enthalpies and entropies of vaporization, corrected to the reference temperatures θ using equations (6) and (7) are presented in Table 9.

$$\Delta_{\mathrm{l}}^{\mathrm{g}} H_{\mathrm{m}}^{\mathrm{o}}(\theta / K) = \Delta_{\mathrm{l}}^{\mathrm{g}} H_{\mathrm{m}}^{\mathrm{o}}(\langle T \rangle) + \Delta_{\mathrm{l}}^{\mathrm{g}} C_{p,\mathrm{m}}^{\mathrm{o}} \cdot \left(\theta - \langle T \rangle\right) \quad (6)$$

$$\Delta_{\mathrm{l}}^{\mathrm{g}} S_{\mathrm{m}}^{\mathrm{o}}(\theta / K) = \Delta_{\mathrm{l}}^{\mathrm{g}} S_{\mathrm{m}}^{\mathrm{o}}(\langle T \rangle) + \Delta_{\mathrm{l}}^{\mathrm{g}} C_{p,\mathrm{m}}^{\mathrm{o}} \cdot \ln(\theta / \langle T \rangle) \quad (7)$$

TABLE 8

Parameters of the Clausius-Clapeyron equation (5) for studies ILs, mean temperature ⟨ *T* ⟩, and pressure *p*(<*T*>) of experimental results. [a]

IL	*A*	*b* / K	r^2	⟨ *T* ⟩ / K	*p*(⟨ *T* ⟩) / Pa
$[C_{14}mim]NTf_2$	30.38 ± 0.05	-16918 ± 27	0.9999	513.06	0.075
$[C_{16}mim]NTf_2$	31.39 ± 0.07	-17694 ± 38	0.9999	520.57	0.074

[a] The uncertainties quoted are the standard deviation of the fitting parameters.

Experimental (*T*, *p*) results were also fitted with the Clarke and Glew equation [21] truncated to the first order:

$$R \cdot \ln \frac{p}{p^{\mathrm{o}}} = -\frac{\Delta_{\mathrm{l}}^{\mathrm{g}} G_{\mathrm{m}}^{\mathrm{o}}(\theta)}{\theta} + \Delta_{\mathrm{l}}^{\mathrm{g}} H_{\mathrm{m}}^{\mathrm{o}}(\theta) \cdot \left(\frac{1}{\theta} - \frac{1}{T}\right) + \Delta_{\mathrm{l}}^{\mathrm{g}} C_{p,\mathrm{m}}^{\mathrm{o}} \cdot \left[\frac{\theta}{T} - 1 + \ln\left(\frac{T}{\theta}\right)\right]. \quad (8)$$

The parameters of the Clarke and Glew equation are presented in table 9. The enthalpies of vaporization were compared to the published values in figure 6. While the results for $[C_{14}mim][NTf_2]$ are in reasonable agreement, the Langmuir and TGA data for $[C_{16}mim][NTf_2]$ are significantly lower than the value from this work [14], [15].

TABLE 9

Parameters of the Clarke and Glew equation (8). Standard (p^o = 0.1 MPa) molar enthalpies $\Delta_l^g H_m^o(\theta)$, entropies $\Delta_l^g S_m^o(\theta)$, and Gibbs energies $\Delta_l^g G_m^o(\theta)$ of vaporization for studied ILs [a]

ΔT/K	θ / K	$\Delta_l^g G_m^o(\theta)$ / kJ·mol^{-1}	$\Delta_l^g H_m^o(\theta)$ / kJ·mol^{-1}	$\Delta_l^g S_m^o(\theta)$ / J·K^{-1}·mol^{-1}	r^2	$\Delta_l^g C_{p,m}^o$ / J·K^{-1}·mol^{-1}
			[C_{14}mim][NTf_2]			
	513.06 [b]	60.2 ± 0.3	140.6 ± 0.2	156.7 ± 0.4		
498 – 528	460.00	67.3 ± 0.3	148.1 ± 0.3	172.2 ± 0.7	0.9999	-176 ± 5 [c]
	298.15	103.2 ± 0.4	178.4 ± 1.1	252.2 ± 2.7		
			[C_{16}mim][NTf_2]			
	520.57 [b]	61.1 ± 0.4	147.1 ± 0.3	165.2 ± 0.6		
508 – 533	460.00	69.9 ± 0.4	156.5 ± 0.4	184.3 ± 0.9	0.9999	-187 ± 5 [c]
	298.15	108.3 ± 0.5	188.7 ± 1.2	269.7 ± 2.9		

[a] The uncertainties quoted are the standard deviation of the fitting parameters. [b] Mean temperature. [c] The $\Delta_l^g C_{p,m}^o$ used in this work are based on the expression that was derived from the experimental $C_{p,m}^o$(l) and derived $C_{p,m}^o$(g) from statistical thermodynamics of the imidazolium [$C_n$mim][NTf_2] series [1], [2], [3], [22].

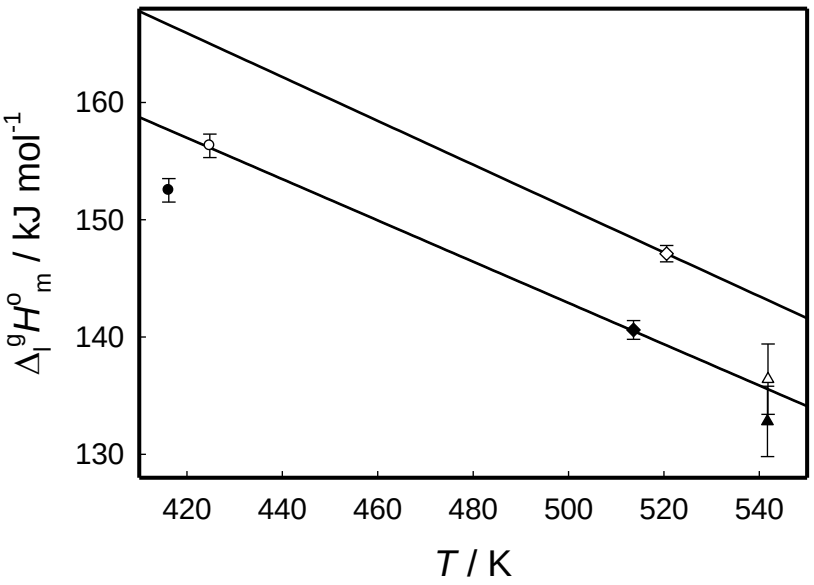

FIGURE 6. Enthalpies of vaporization for $[C_{14}mim][NTf_2]$ (filled symbols) and $[C_{16}mim][NTf_2]$ (hollow symbols): diamonds, KEQCM from this work; circles, quartz-microbalance Langmuir method [14]; triangles, TGA [15]; ——, values extrapolated using $\Delta_l^g C_{p,m}^o$ from table 10.

4. Discussion

The dependence of heat capacity on the alkyl chain length is presented in figure 7. The data refer to T = 320 K at which the compounds studied are liquid. The dependence is linear within the uncertainties. The maximum deviation does not exceed 4 $J \cdot K^{-1} \cdot mol^{-1}$ for $n \leq 16$. The value for n = 18 [5] is about 20 $J \cdot K^{-1} \cdot mol^{-1}$ high relative to the general trend. The reason of this deviation is unknown.

Similar behaviour was observed for the liquid-phase entropy (figure 8). The maximum deviation from the straight line was 3 $J \cdot K^{-1} \cdot mol^{-1}$.

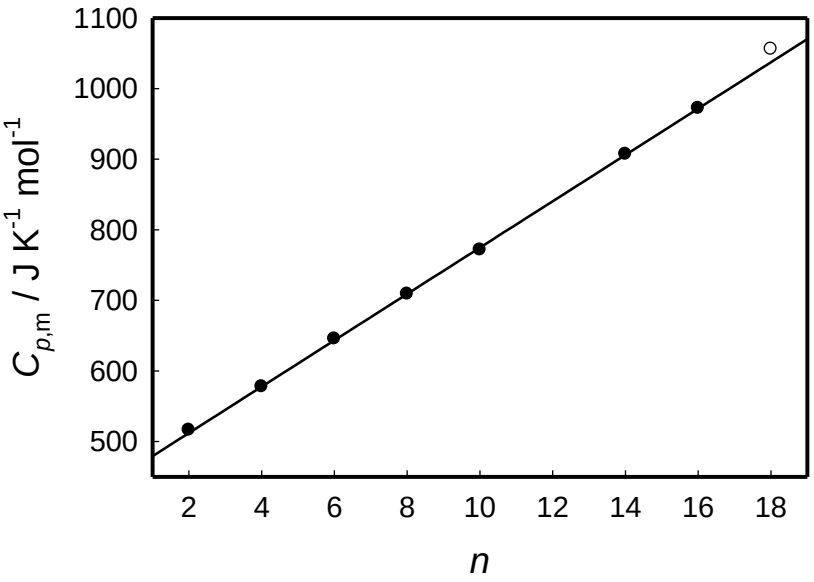

FIGURE 7. Isobaric heat capacity of liquid [C$_n$mim][NTf$_2$] at T = 320 K as a function of n. The value for n = 18 was estimated from the plot [5], the data for n = 2–8 were taken from Refs. [1], [2], [3].

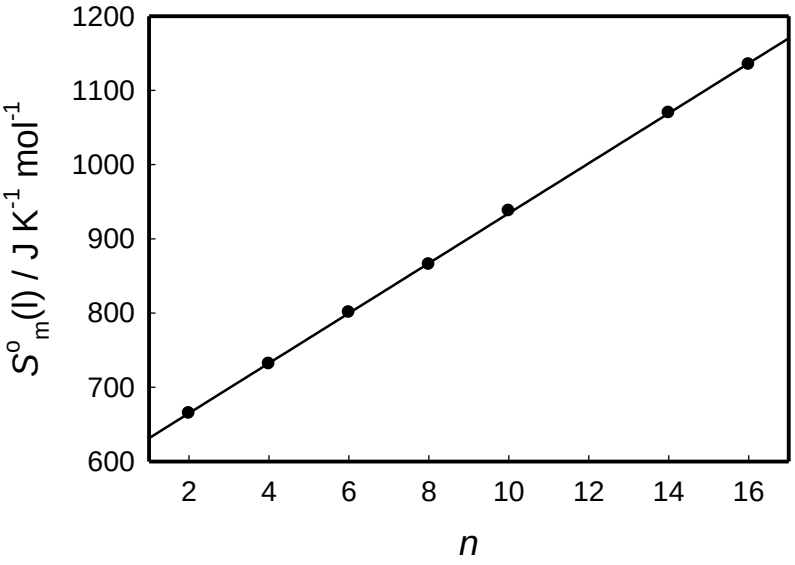

FIGURE 8. Entropy of liquid [C$_n$mim][NTf$_2$] at T = 320 K as a function of n. The data for n = 2–8 were taken from Refs. [1], [2], [3]. The value for n = 4 considers the residual entropy of the crystal [23].

The solid-liquid phase change entropy $\Sigma\Delta_{tr}S_m$ is a sum of entropies of solid-phase transitions and fusion. This quantity demonstrates non-linearity for the [C$_n$mim][NTf$_2$] series (figure 9). The value for n = 18, $\Sigma\Delta_{tr}S_m$ = 237 J·K^{-1}·mol^{-1} [5], is significantly higher than the value ≈200 J·K^{-1}·mol^{-1} predicted based on the results of this work. The difference is probably caused by a different procedure for selecting the heat-capacity baseline for fusion in Ref. [5] relative to this work. Experimental values were not reported in Ref. [5], so an independent calculation cannot be made. The $\Sigma\Delta_{tr}S_m$ vs. n dependence for the polymorphic sequences with the highest T_{fus} for each compound is described by the equation:

$$\Sigma\Delta_{tr}S_m / \text{J·K}^{-1}\text{·mol}^{-1} = 71.2 + 4.40n + 0.1424n^2 \qquad (9)$$

The outlier is [C$_{10}$mim][NTf$_2$] whose $\Sigma\Delta_{tr}S_m$ deviates from eq. (9) by 19 J·K^{-1}·mol^{-1}.

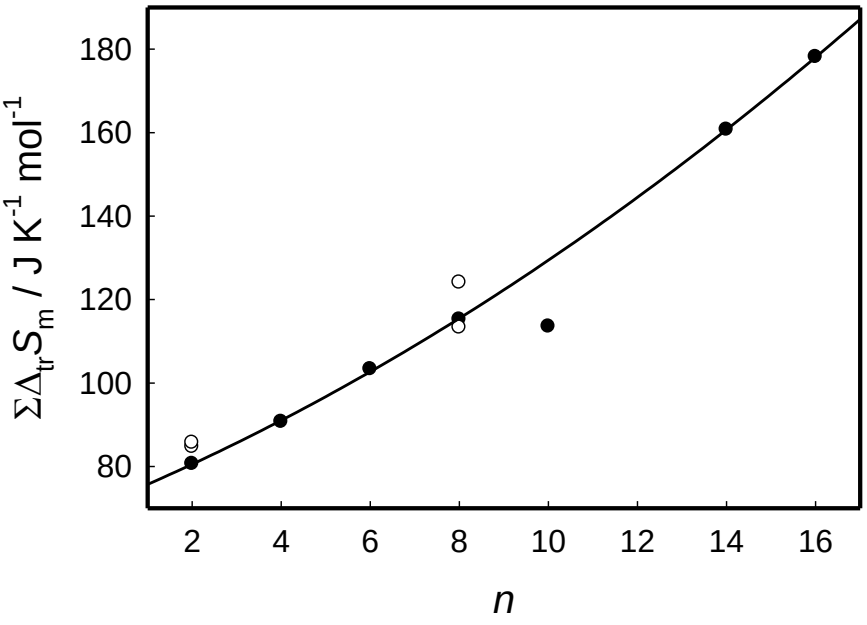

FIGURE 9. Solid-liquid phase-change entropies of [C$_n$mim][NTf$_2$] as a function of n. ●, polymorphic sequences with highest T_{fus}; ○, polymorphic sequences with lower T_{fus}.

The enthalpies of vaporization for the considered series of ILs are compared in figure 10. At short alkyl chain length, the enthalpies of vaporization decrease with the increase of the alkyl

chain length, at large *n*, the dependence becomes linear. Similar behaviour was observed for the standard entropies of vaporization.

The obtained results allowed us to calculate ideal-gas entropies $S^{o}_{m}(g)$ at T = 460 K for the even [C$_n$mim][NTf$_2$] ILs up to n = 16 using the equation:

$$S^{o}_{m}(g) = S^{o}_{m}(l) + \frac{\Delta^{g}_{l}H^{o}_{m}}{T} + R\ln\frac{p}{p^{\circ}}. \qquad (10)$$

where p° = 0.1 MPa.

The liquid heat capacities were extrapolated to T = 460 K using the liquid heat-capacity equations from the corresponding works. This quantity was found to be a linear function of n (figure 11). Deviations from the line do not exceed 9 J·K^{-1}·mol^{-1} thus indicating that the expanded uncertainty of these values is $U_r(S^{\circ}_m)$ = 0.7% (0.95 confidence interval).

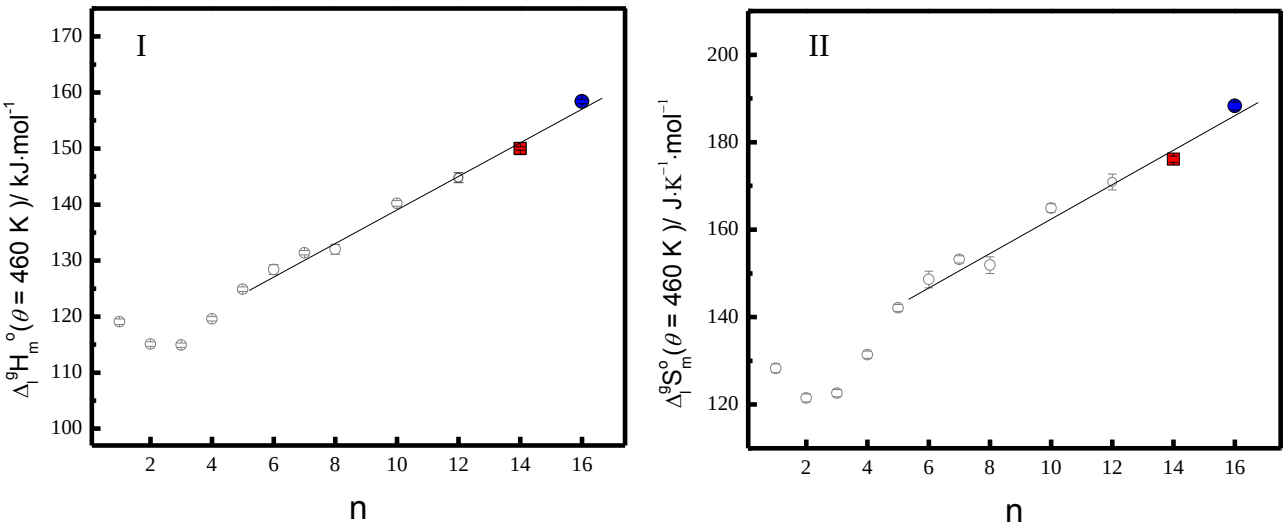

FIGURE 10. Graphical representation of the standard (p° = 0.1 MPa) molar enthalpies $\Delta^{g}_{l}H^{o}_{m}$ (θ = 460.0 K) (**I**) and entropies $\Delta^{g}_{l}S^{o}_{m}$ (θ = 460.0 K) (**II**) of vaporization for the ionic liquids as a function of the number of carbons n(C) in the alkyl chain of the cation. This work: ■ [C$_{14}$mim][NTf$_2$], ● [C$_{16}$mim]NTf$_2$]; ○, literature data for [C$_n$mim]NTf$_2$] [12], [13] (with n = 1 to 12).

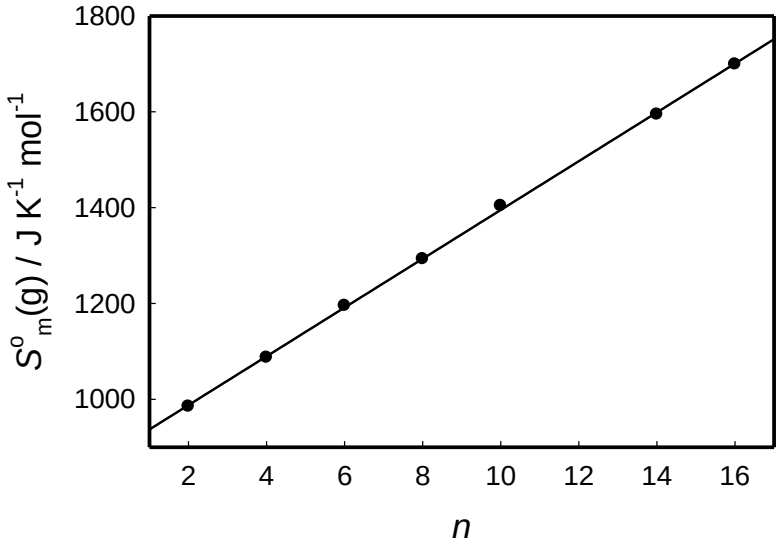

FIGURE 11. Standard entropies of [C$_n$mim][NTf$_2$] in the ideal-gas state at T = 460 K as a function of n. Straight line is a function $S°_m$ / J·K^{-1}·mol^{-1} = 886.3 + 50.87n.

5. Conclusion

The heat capacities and phase-transition properties in the condensed state were determined for three [C$_n$mim][NTf$_2$] (n = 10, 14, 16) ILs. All compounds were found to have solid-phase transitions. Vapour pressures of [C$_{14}$mim][NTf$_2$] and [C$_{16}$mim][NTf$_2$] were measured by the KEQCM technique, and the thermodynamic parameters of vaporization were derived. Results were combined with those available in the literature for the short-chain homologues to demonstrate regularities in thermodynamic properties of the series. Some properties (molar heat capacity in the liquid state, standard molar entropy in the gas state) were found to change linearly with the alkyl chain length, while the more complicated behaviour was observed for the thermodynamic parameters of vaporization and the total solid-liquid phase change entropies. The trend shift at the critical alkyl size n = 6 reported earlier [12] for the enthalpies and entropies of vaporization is confirmed by the present results (figure 10). The

break at n = 6 was observed previously in the surface tension and viscosity [24], [25] and in other properties [26], [27], [28], [29]. To provide better detection of the trend change, the complete alkyl series from n = (1 to 10) including odd and even number of carbons were used.

Acknowledgements

This work was supported by the Belarusian State Program of Scientific Research «Chemical technologies and materials, natural resource potential» (grant 1.35) and Fundação para a Ciência e Tecnologia (FCT), Lisbon, Portugal and to FEDER for financial support to Centro de Investigação em Química, University of Porto through the project Pest-C/QUI/UI0081/2011 and PTDC/aac-amb/121161/2010, Ana S. M. C. Rodrigues acknowledge the financial support from Fundação para a Ciência e a Tecnologia for the award of research grant with reference, SFRH/BD/81261/2011. Thanks are due to the support from the COST Action CM1206. Eugene Paulechka and Andrey Blokhin are grateful to Aliaksei Strechan for his help in calorimetric measurements on $[C_{14}mim][NTf_2]$.This article is, in part, a contribution of NIST, and is not subject to copyright in the United States for the author E. P. Trade names are provided only to specify procedures adequately and do not imply endorsement by the National Institute of Standards and Technology. Similar products by other manufacturers may be found to work as well or better.

Appendix A. Supplementary data

Supplementary data associated with this article can be found, in the online version, at

References

[1] Y. U. Paulechka, A. V. Blokhin, G. J. Kabo and A. A. Strechan, J. Chem. Thermodyn. 39 (2007) 866-877.

[2] A. V. Blokhin, G. J. Kabo and Y. U. Paulechka, J. Chem. Eng. Data 51 (2006) 1377-1388.

[3] A. V. Blokhin, Y. U. Paulechka, A. A. Strechan and G. J. Kabo, J. Phys. Chem. B 112 (2008) 4357-4364.

[4] Y. Shimizu, Y. Ohte, Y. Yamamura, K. Saito and T. Atake, J. Phys. Chem. B 110 (2006) 13970–13975.

[5] Y. Shimizu, Y. Ohte, Y. Yamamura and K. Saito, Chem. Phys. Lett. 470 (2009) 295-299.

[6] Y. Shimizu, Y. Ohte, Y. Yamamura, S. Tsuzuki and K. Saito, J. Phys. Chem. B 116 (2012) 5406-5413.

[7] M. Rocha, M. Bastos, J. Coutinho and L. Santos, J. Chem. Thermodyn. 53 (2012) 140-143.

[8] L. Santos, M. Rocha, A. Rodrigues, V. Stejfa, M. Fulem and M. Bastos, J. Chem. Thermodyn. 43 (2011) 1818-1823.

[9] S. V. Dzyuba, R. A. Bartsch, ChemPhysChem 3 (2002) 161-166.

[10] A. E. Bradley, C. Hardacre, J. D. Holbrey, S. Johnson, S. E. J. McMath, M. Nieuwenhuyzen, Chem. Mater. 14 (2002) 629-635

[11] T. Li, F. Xu, W. Shi, Chem. Phys. Lett. 628 (2015) 9-15

[12] M. A. A. Rocha, C. F. R. A. C. Lima, L. R. Gomes, B. Schröder, J. A. P. Coutinho, I. M. Marrucho, J. M. S. S. Esperança, L. P. N. Rebelo, K. Shimizu, J. N. Canongia Lopes and L. M. N. B. F. Santos, J. Phys. Chem. B 115 (2011) 10919-10926.

[13] M. Rocha, F. Ribeiro, B. Schröder, J. Coutinho and L. Santos, J. Chem. Thermodyn. 68 (2014) 317–321.

[14] D. Zaitsau, S. Verevkin, V. Emel'yanenko and A. Heintz, Chem. Phys. Chem. 12 (2011) 3609-3613.

[15] S. Verevkin, D. Zaitsau, V. Emel'yanenko, R. Ralys, A. Yermalayeu and C. Schick, J. Chem. Thermodyn. 54 (2012) 433-438.

[16] F. Pavese and V. M. Malyshev, Adv. Cryog. Eng. 40 (1994) 119-124.

[17] "Fundamental Physical Constants - Physico-chemical constants," [Online]. Available: http://physics.nist.gov/constants. [Accessed 26 October 2015].

[18] L. M. N. B. F. Santos, L. M. S. S. Lima, C. F. R. A. C. Lima, F. D. Magalhães, M. C. Torres, B. Schröder and M. A. V. Ribeiro da Silva, J. Chem. Thermodyn. 43 (2011) 834–843.

[19] Y. U. Paulechka, A. G. Kabo, A. V. Blokhin, G. J. Kabo and M. P. Shevelyova, J. Chem. Eng. Data 55 (2010) 2719-2724.

[20] A. V. Blokhin, Y. U. Paulechka and G. J. Kabo, Thermochim. Acta 445 (2006) 75-77.

[21] E. Clarke and D. Glew, Trans. Faraday Soc. 62 (1966) 539-547.

[22] Y. U. Paulechka, G. J. Kabo and V. N. Emel'yanenko, J. Phys. Chem. B 112 (2008) 15708–15717.

[23] Y. U. Paulechka, G. J. Kabo, A. V. Blokhin, A. S. Shaplov, E. I. Lozinskaya, D. G. Golovanov, K. A. Lyssenko, A. A. Korlyukov and Y. S. Vygodskii, J. Phys. Chem. B 113 (2009) 9538-9546.

[24] H. Almeida, M. Freire, A. Fernandes, J. Lopes-da-Silva, P. Morgado, K. Shimizu, E. Filipe, J. Canongia Lopes, L. Santos and J. Coutinho, Langmuir 30 (2014) 6408-6418.

[25] A. Rodrigues, M. Rocha, H. Almeida, C. Neves, J. Lopes-da-Silva, M. Freire, J. Coutinho and L. Santos, J. Phys. Chem. B 119 (2015) 8781–8792.

[26] M. Vilas, M. Rocha, A. Fernandes, E. Tojo and L. Santos PhysChemChemPhys, 17 (2015) 2560-2572.

[27] M. Rocha, J. Coutinho and L. Santos, J. Chem. Phys. 141 (2014) 134502.

[28] C. Bernardes, K. Shimizu, A. Ferreira, L. Santos and J. Canongia Lopes, J. Phys. Chem. B 118 (2014) 6885-6895.

[29] M. Rocha, J. Coutinho and L. Santos, J. Chem. Phys. 139 (2013) 104502.